

Atmospheric Limitations to Repeat-track Radar Interferometry

Richard Goldstein

Jet Propulsion Laboratory

Pasadena, CA 911.09

May 1, 1995

Heading

In its recent radar imaging mission, the Shuttle Imaging Radar satellite (SIR-C) devoted three days to repeat-track interferometry. We have analyzed the data from a test site in the Mojave desert of California. Although good topography (± 10 m on 21 m postings) was obtained, most of the error was caused by turbulent water vapor in the lower atmosphere. Spatial structure of 6 km and all smaller sizes was observed. The RMS, one-way time delay was found to be .24 cm. Essentially identical results were obtained at two wavelengths, 24 and 5.7 cm.

Introduction

The earliest application of interferometry to radar was by Rogers and Ingalls (ref 1), to remove an ambiguity in radar echoes from the planet Venus. For such distant reflectors there are, in general, two places on the surface that have the same range and the same range rate, the so-called north/south ambiguity. In that work, surface topography was assumed to be zero.

The earliest application of interferometry to topography was by Zisk (ref. 2), who, for the case of the Moon, had enough antenna directivity to avoid the ambiguity. Later, Graham (ref. 3) applied interferometry to an aircraft radar to obtain contours of interference, related to topography.

All of the above work employed two antennas, simultaneously, to form the interferograms. It is possible, however, to use one antenna at two different times to serve the same purpose. The first demonstration of two-pass interferometry was by Li and Goldstein (ref. 4), who studied topography construction via the multiple baselines afforded by the Seasat radar satellite.

For successful two-pass interferometry, two conditions must be met. The satellite (or aircraft) must return closely enough to its original position so that coherence is obtained (usually closer than 500 m) , and the surface must not have been unduly disturbed during the time between observations. If the surface is perturbed too much, coherence will be lost; if moved only slightly, the topography can still be in error.

There is much current activity in obtaining topography by two-pass interferometry, employing data from the European satellite ERS-1, the US satellite SIR-C, and the soon to be launched Canadian satellite RADARSAT. We study here the effects of Earth's ionosphere and/or troposphere on topographic accuracy, as revealed by adding a third pass to the data set.

Given a third observation, two interferograms can be formed. It is the small inconsistencies between the two interferograms that are of interest here. Gabriel and Goldstein (ref. 5) have used three-pass interferometry from Seasat data to detect surface motions of less than a centimeter for irrigated fields in the Imperial Valley of California. For this work, we apply the technique to a region of the Mojave desert of California, where little was expected to change in the interval between observations . This desert is high, very dry, and except for an

occasional earthquake, is among the world's most stable areas.

The Space Shuttle

The Shuttle Imaging Radar (SIR-C) was launched on September 30, 1994, on a ten day mission. Its primary task was to investigate a large number of sites with synthetic aperture radar, at three different wavelengths and a number of polarization combinations. The last three days were devoted to an experiment to repeat as precisely as possible a single ground track, for multi-pass interferometry. The repeat tracks were separated by 23 min less than 24 hours.

The Shuttle navigation turned out to be superb, resulting in some baselines within a few dozens of meters. For our site, the components of the two baselines perpendicular to the line-of-sight were contained within 67 meters. The data were taken on October 7, 8 and 9, 1994, at the end of the long, hot summer.

The **Data Set**

We have for study three radar observations of the same site, each at two wavelengths, 24 cm and 5.7 cm. The radar images have slant-range resolution of 3.3 m and along track resolution of 5.2 m. We have averaged 16 adjacent pixels to give a ground resolution, and pixel spacing, of **21**.m in both directions.

Figure 1 is a print of a 24 cm wavelength image, 21.4 km by 18.8 km. North is marked on the figure. The Shuttle flight line is downward, along the left edge of the figure. The angle of incidence of the radiation was 42°. Because this image has not been corrected for topography, the mountain peaks appear to lean to the left - the "layover" phenomenon of radar images, which have slant range as one of the coordinates.

To form an interferogram, two images are co-registered and an image of the phase difference between corresponding pixels is created. Figure two is such an interferogram for the 24 cm images, with an inset of the shorter wavelength, of October 7 and 9. As can be seen from the figure, the correlation is excellent; the surface changed little in the two intervening days.

Layover is much more prominent in the fringes of the 5.7 cm inset of figure 2. On some of the mountain peaks, fringes from greater heights actually cross over lower ones.

If the baseline is accurately known, the phases of figure 2 can be used to determine the topography. We have used 7 tie-points from a published map of the area to solve, in the least squares sense, for the baseline. The resulting altitudes are presented in figure 3, where one color fringe represents a height change of 200 m. Layover has been corrected in figure 3. A radar brightness image, at low contrast, has been superimposed on the figure.

Three-Pass

The geometry of the three observations is given in figure 4. The plane of the page is represented as perpendicular to the SIR-C orbits, which are shown moving out of the page. B_{12} and B_{13} are the baselines, separated by the angle α . θ is a function of the topography, ρ is the slant range and the d_i are possible delays caused by the Earth's ionosphere or troposphere.

The three phases observed for the pixel of figure 4 are:

$$\begin{aligned}
 \phi_1 &= \frac{4\pi}{\lambda} (\rho + d_1) \\
 \phi_2 &= \frac{4\pi}{\lambda} (\rho + d_2 - B_{12} \cos(\theta + \alpha)) \\
 \phi_3 &= \frac{4\pi}{\lambda} (\rho + d_3 - B_{13} \cos(\theta))
 \end{aligned}
 \tag{1}$$

The phases of the two interferograms are simply the differences :

$$\begin{aligned}
 \phi_{12} &= \frac{4\pi}{\lambda} (B_{12} \cos(\theta + \alpha) + d_1 - d_2) \\
 \phi_{13} &= \frac{4\pi}{\lambda} (B_{13} \cos(\theta) + d_1 - d_3)
 \end{aligned}
 \tag{2}$$

When θ is eliminated from equation 2, and the extra delays are neglected, the curve of ϕ_{12} versus ϕ_{13} is an ellipse. Only a small arc of the ellipse is significant since the excursion of θ is limited to only 3.3° by the swath width. The extra (atmospheric) time delays are revealed by the measured points not falling on the ellipse.

The Troposphere

Following the method of ref(5), we have fitted a quadratic function (in lieu of an arc of an ellipse) to the phase data for the two 5.7 cm interferograms, and present the residuals of the fit in figure 5. The peak-to-peak variation in residual time delay (1-way) is about 2.8 cm; the RMS, about 0.3 cm.

A similar fit made to the 24 cm data produces a result that is all but indistinguishable from figure 5. Since there is no frequency dispersion in the observed effect, we conclude that the ionosphere cannot be responsible. It must be the troposphere .

It is likely that the extra delay features of figure 5 are the results of water vapor and turbulence in the troposphere. The features show little, if any, correlation with the topography of the area (shown in figure 3), so they are not confined to ground level.

A spatial spectrum of the delay features is given in figure 6, where a line with $-8/3$ slope which, is a characteristic of turbulence (ref. 6), is marked on the spectrum. The departure from the $-8/3$ slope at about 1 cycle per 6 km shows the scale height of the phenomenon; the departure at 1 cycle per 0.4 km shows where the radar phase noise begins to dominate the effect.

The residuals of figure 5 are the result of the tropospheric disturbances of three separate days. From the fit of ϕ_{12} versus ϕ_{13} , it follows that:

$$\phi_{12} = C + S\phi_{13} \quad (3)$$

where C is the constant and S is the slope of the fit. The quadratic term is very small and has no effect on the analysis to follow.

The tropospheric induced residuals would then be:

$$\begin{aligned} e &= \Delta\phi_{12} - s\Delta\phi_{13} \\ e &= d_1 - d_2 - s(d_1 - d_3) \\ \langle e^2 \rangle &= \langle d_1^2 \rangle (1-s)^2 + \langle d_2^2 \rangle + s^2 \langle d_3^2 \rangle \end{aligned} \quad (4)$$

where the brackets $\langle . \rangle$ indicate average, and the separate days are assumed independent.

If the effects of each day are of the same magnitude, which we discuss below, then:

$$\sigma_{\phi} = \frac{\sigma_e}{\sqrt{2(s^2 - s + 1)}} \quad (5)$$

Application of equation 5 leads to an RMS path length variation of .24 cm for each day of the observations. Such a variation in effective path length maps into an error of 6.7 m RMS for our elevation estimates. Larger baselines would lead to smaller errors; shorter ones would lead to greater.

Global Positioning Satellite Data

We are fortunate to have available GPS tracking data (ref. 7) from within a few km of the radar site. Satellite GPS28 overflew the area within 30 min of SIR-C, and at almost the same elevation angle, but at a different track angle. The RMS residuals of the time delays for the three days in question are .57, .53 and .58 cm.

The data were sampled every 5 min and are largely uncorrelated. These values are larger than the SIR-C results, above, which can be expected since the GPS28 altitude is much higher. GPS28 orbits at an altitude of about 20,000 km; SIR-C was at about 210. The preponderance of the Earth's ionosphere was above SIR-C, but below GPS28.

Water Vapor Radiometer Data

We are also fortunate to have available data from a water vapor radiometer close to the radar site and at the times of the SIR-C overflights (ref. 8). The radiometer measured zenith radio temperatures at a wavelength of 1.45 cm. The temperatures are

related to an integrated column of water vapor, which in turn are related to residual time delays.

These residuals were sampled every 4.2 rein, and, except for the first day, are also uncorrelated. The RMS results for the three days are .37, .23 and .24 cm - very close to the radar result. The larger variation on the first day appears to be caused by a steady change in the water vapor content over several hours, an effect that would be unnoticed by the radar.

Conclusions

Tropospheric turbulence, coupled with water vapor content, appears to limit the accuracy of motion detection and topographic estimation by two-pass radar interferometry.

For our test site in the Mojave desert, the tropospheric time delay errors were .24 cm. The RMS error caused by receiver and baseline noise was much less, .046 cm at 5.7 cm wavelength. For more humid locations, the tropospheric error can be expected to be greater.

We note that this limit does not apply if interferometry is performed with two antennas, simultaneously.

Acknowledgements

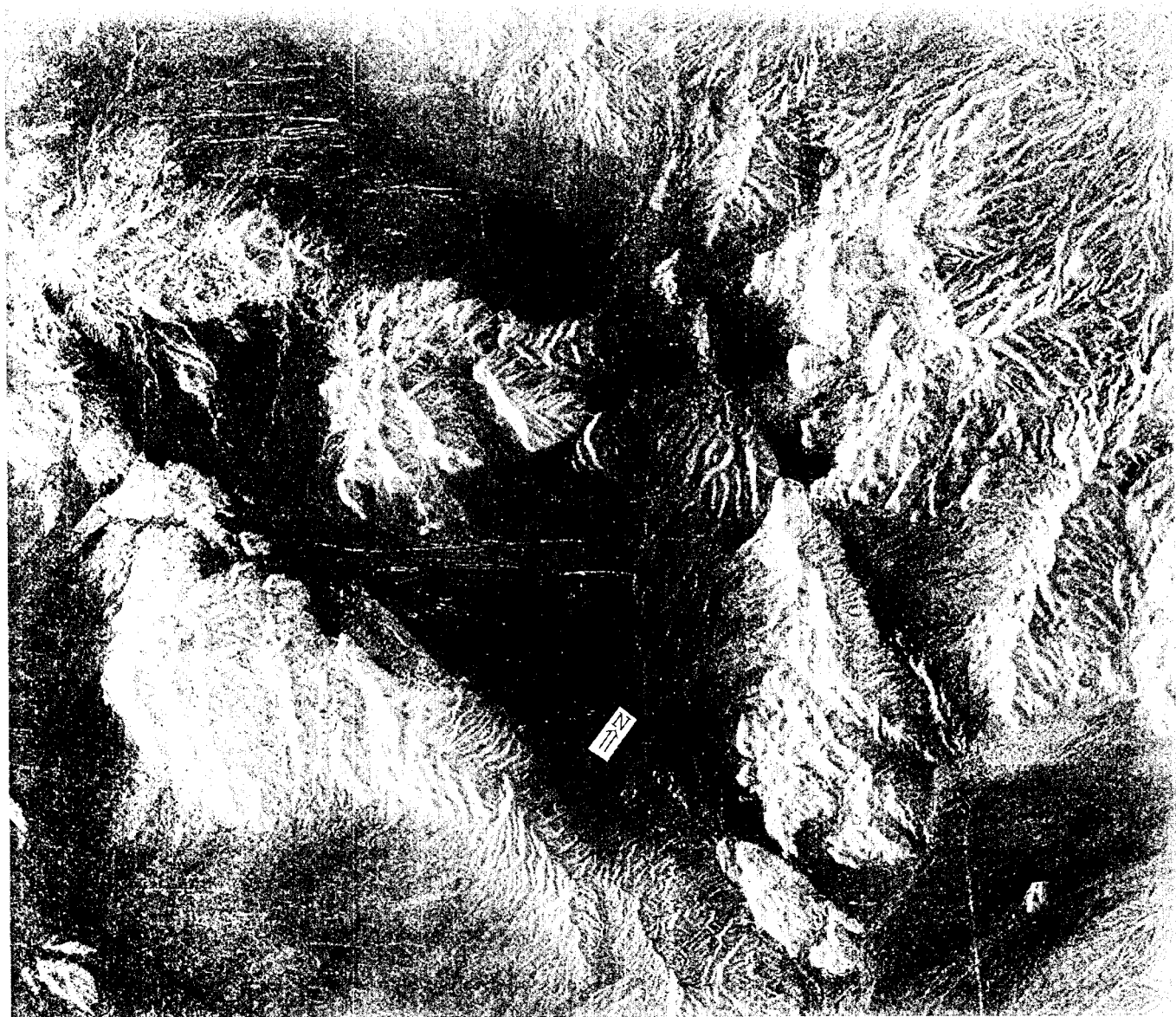
The research described in this paper was carried out by the Jet Propulsion Laboratory, California Institute of Technology, under a contract with the National Aeronautics and Space Administration .

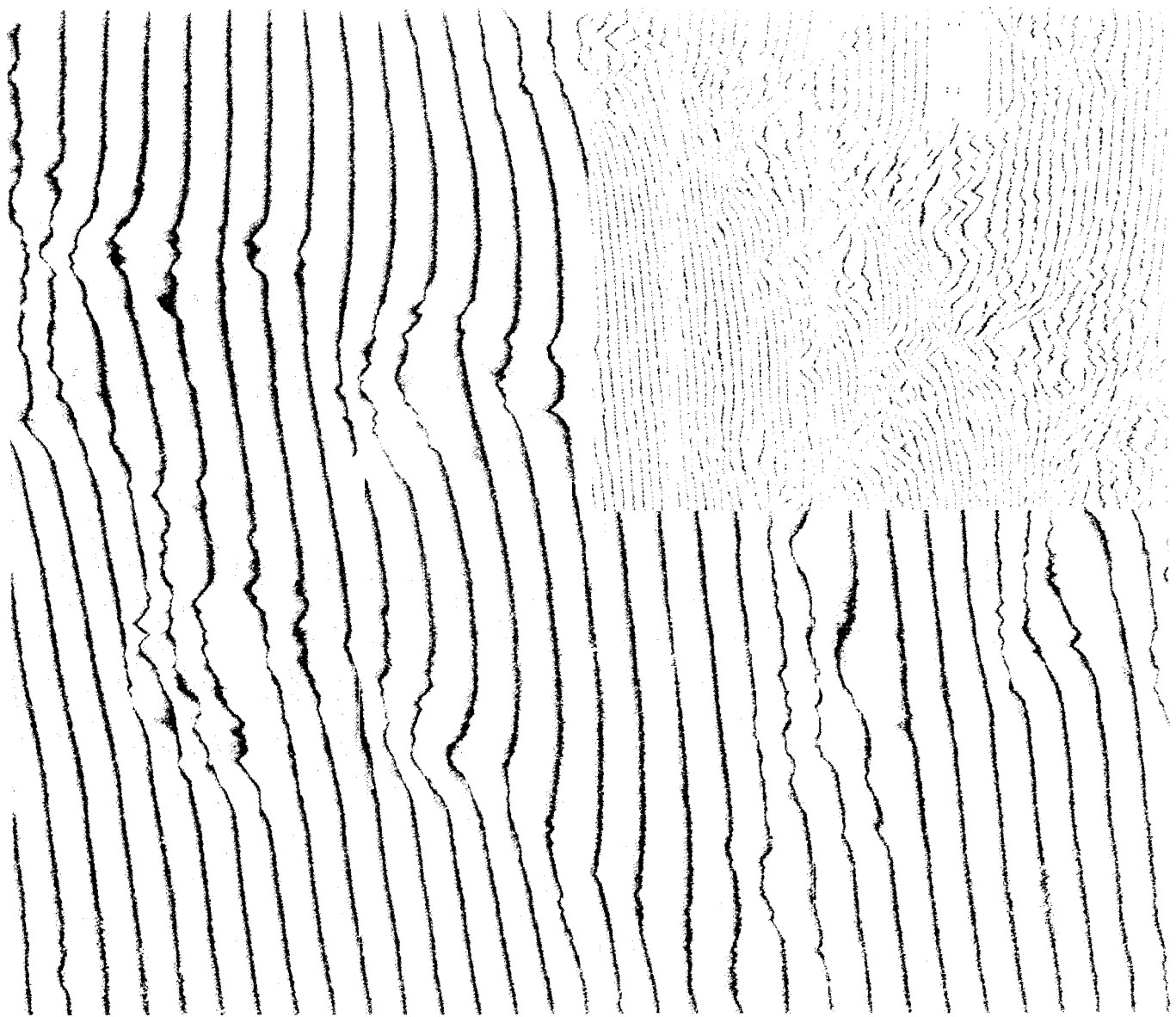
References

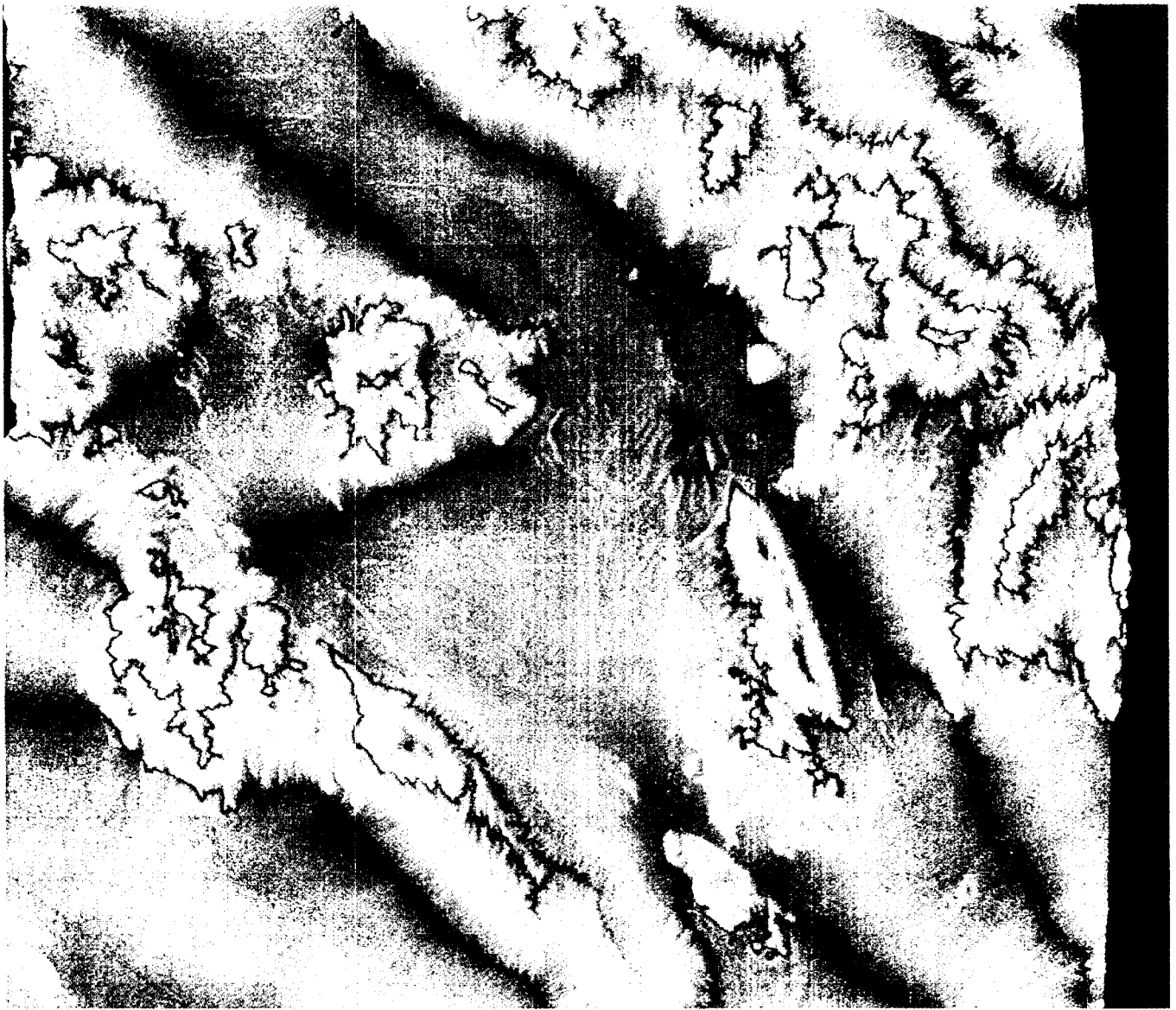
- 1) Rogers, A. E. E. and R. p. Ingalls, "Venus: mapping the surface reflectivity by radar interferometry", *Science*, vol. 165, pp. 797-799, 1969.
- 2) Zisk, S. H., "A new, Earth-based radar technique for the measurement of lunar topography", *Moon*, vol. 4, pp. 296-300, 1972a.
- 3) Graham, L. C., "Synthetic interferometric radar for topographic mapping", *Proc. IEEE*, vol. 62, pp. 763-768, June, 1974.
- 4) Li, F. K. and R. M. Goldstein, "Studies of multibaseline spaceborne interferometric synthetic aperture radars", *IEEE Trans Geoscience and Remote Sensing*, Vol. 28, no. 1, pp. 88-97, Jan. 1990.
- 5) Gabriel, A. K., and R. M. Goldstein, "Mapping small elevation changes over large areas: differential radar interferometry", *J. of Geophysical Research*, vol. 94, no. B8, pp. 9183-9191, July 10, 1989.
- 6) Tatarskii, V. I., "Wave propagation in a turbulent medium", *Dover, New York*, 1961.
- 7) Jefferson, D, Y. Bar-Sever, C. Dunn, M. Helfin, K. Hurst, R. Muellerschoen, Y. Vigue, M. Watkins, F. Webb and J. Zumberge, "The effects of anti-spoofing on routine global GPS analysis", *AGU meeting, San Francisco, CA, Fall, 1994*.
- 8) Keihm, S. , Jet Propulsion Laboratory, personal communication .

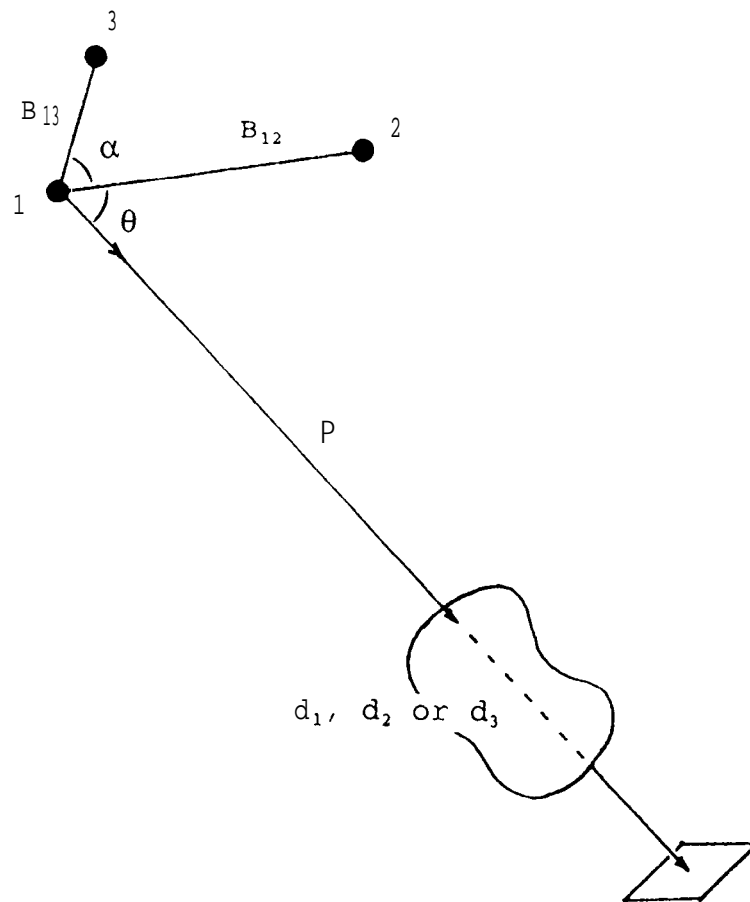
Figures

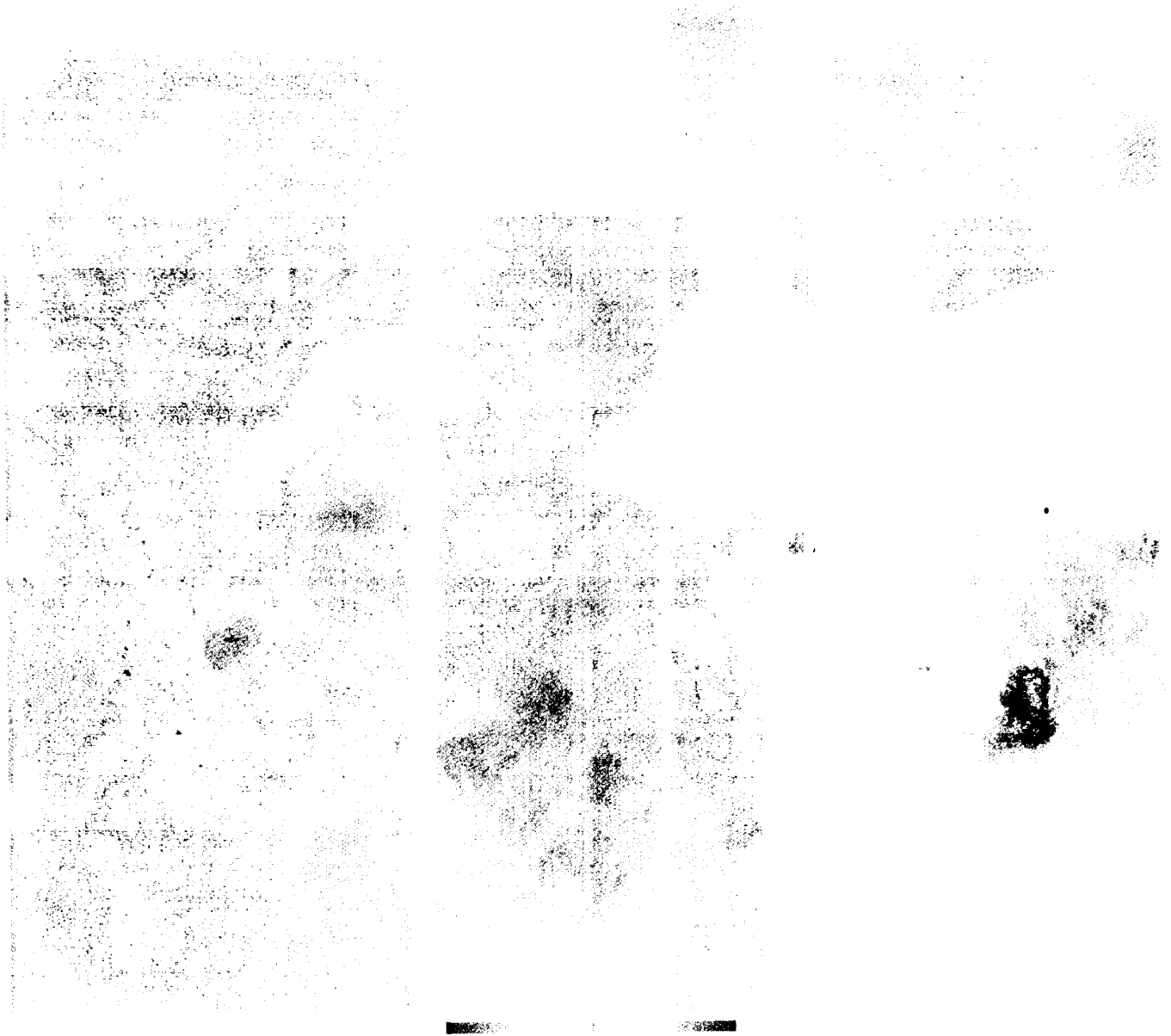
- 1) Conventional radar image of test site in the Mojave desert of California. Image is 21.4 by 18.8 km; resolution is 21 m. Radar wavelength is 24 cm.
- 2) Radar interferogram of same area as figure 1. Phase is encoded as color, each fringe represents 12 cm (2.8 cm in the inset) difference in slant range between two observation points. Fringes are 4.3 times more dense on the corresponding interferogram of 5.7 cm wavelength.
- 3) Elevation map derived from the shorter wavelength interferogram. Each fringe represents elevation contours. They are separated by 200 m. Layover has been corrected in this image.
- 4) Geometry of three-pass interferometry. Three positions of SIR-C, on three separate days, are shown. The line-of-sight is to one particular resolution element. Tropospheric delays are shown schematically.
- 5) An image of phase inconsistencies, attributed to water vapor turbulence. The same color code is used as in figure 2. One fringe represents 2.8 cm of anomalous time delay, spread over the three days.
- 6) Power spectrum of the data presented in figure 5. The added line follows the $-8/3$ slope to be expected from radar through a turbulent atmosphere containing water vapor.











Time Delay

